JOURNAL OF SOLID STATE CHEMISTRY **137,** 71–76 (1998)
ARTICLE NO. SC977691

Phase Transition and Structure of a $K_{1-x}Li_xMnF_3$ Single Crystal in the Range 100–298 K

A. Waśkowska

Institute of Low Temperature and Structure Research, Polish Academy of Sciences, 50 950 Wrocław, Poland

and

A. Ratuszna

Institute of Physics, University of Silesia, 40 007 Katowice, Poland

Received August 25, 1997; in revised form October 30, 1997; accepted October 31, 1997

The cubic-to-tetragonal phase transition in the mixed perovskite $K_{1-x}Li_xMnF_3$ ($x < 0.036$) was investigated by single-crystal X-ray diffraction. Results of the structure refinement at 298 and 145 K are discussed. They confirm the cubic symmetry, the space group *Pm3m*, of the room temperature phase with strongly anisotropic thermal vibration amplitudes of the F atoms, which were also observed in the parent $KMnF_3$. Substitutional lattice imperfections at the K^+ sites shift the ferrodistortive phase transition to higher temperature $T_{c1} = 191$ K, compared to 186.5 K in $KMnF_3$. The structural changes in the tetragonal phase (*I4/mcm*) are characterized by the displacements of the F atoms from the positions they occupy above T_{c1}. However, the Li^+ ion dopants do not affect the octahedral network, the MnF_6 octahedra remain regular, and no displacements of K^+/Li^+ cations along the tetragonal *c* axis are observed. The thermodynamic character of the transition is illustrated with the critical behavior of the unit cell parameters and the temperature-dependent evolution of the tetragonal deformation and the macroscopic strain. A variation of the integrated intensity of superstructure reflections close to T_{c1} has been assumed to describe the behavior of the order parameter. As far as the precision of the present experiment allows, all these observations show that 3.6% Li^+ substitution at the K^+ site does not radically change the nature of the transition in $KMnF_3$ at T_{c1}.

INTRODUCTION

Perovskite compounds ABX_3 show one of two types of distortion from the cubic structure when the temperature is lowered. Either the *B* atom moves off-center in its octahedron to give a ferroelectric phase ($BaTiO_3$) or the BX_6 octahedra rotate to change the number of *X* atom bonds to *A* ($SrTiO_3$) (e.g., refs 1–3).

$KMnF_3$ belongs to the second type of perovskites and shows a sequence of structural and magnetic transitions from the parent cubic to tetragonal ($T_{c1} = 186$ K) → orthorhombic ($T_{c2} = 88$ K) → tetragonal ($T_{c3} = 82$ K) phases which are related to the dynamics of the MnF_6 octahedra (e.g., refs 4–7). The mechanism of the transition has been described in a number of papers (8–10). It has also been shown that the structural and physical properties of $KMnF_3$ can be essentially changed by some amount of substitutional ions introduced either at the K^+ or at the Mn^{2+} ion site (8, 10–13). The concentration and ionic radii of the substituents influence the temperature and the mechanism of the transition.

In the course of our systematic studies of perovskite fluorides with 3*d* transition metals, we have investigated the mixed compound $K_{1-x}Li_xMnF_3$ ($x = 0.005$ and 0.01) to examine the temperature-dependent sequence of the phase transitions in the crystal, which can be considered to contain lattice defects (12). The present paper describes the structural phase transition at $T_{c1} = 191$ K for the crystal with the Li^+ cation ($x \approx 0.04$) introduced into the *A* interstices formed by a network of corner-shared MnF_6 octahedra and in the parent compound occupied by the dodecahedrally coordinated K^+ ions. From the ionic radii of $Li^+ = 1.15$ Å and $K^+ = 1.64$ Å (14), one can expect that a size effect will play some role in the thermodynamic character of the transition.

Using the X-ray diffraction technique, we determined the structure of the single crystal at room temperature and at 145 K in the context of the structural transition at T_{c1} in the parent $KMnF_3$. The transition characteristics will also be discussed by means of the critical behavior of the unit cell parameters, spontaneous strain, and integrated intensity of superlattice reflections in the temperature range 150–200 K.

0022-4596/98 $25.00

EXPERIMENTAL

1. Crystal Growth and Data Collection

$K_{1-x}Li_xMnF_3$ was grown by the Bridgman method (15). The stoichiometric ingredients, $(1-x)KF + xLiF + MnF_2$ (Aldrich Reagent Inc.), were melted at 1050°C in a graphite crucible under an argon atmosphere for 40 hr. A sample of almost perfect cubic shape with dimensions $0.12 \times 0.13 \times 0.12$ mm was cut from a bulk crystal with a volume of several cubic centimeters. The quality of the single crystal was tested with rotation and Weissenberg photographs. The intensity data collection was performed on a Kuma KM-4 diffractometer (κ-geometry, Mo$K\alpha$ radiation, graphite monochromator) using the ω–2θ scan mode. Two structural data sets were collected: at room temperature and below T_{c1} at 145 K. Integrated intensities for all measured reflections were calculated using a profile analysis program, allowing the weak and polydomain reflections to be evaluated more accurately (16). The integrated intensities were corrected for Lorentz–polarization factors and absorption (analytical correction). For low-temperature measurement (90–298 K), a cold nitrogen gas stream attachment (Oxford Cryosystem) was used (17). The stability of temperature was $\sim$1 K. The transition temperature was monitored by looking for the splitting of the $(004)_c$ reflection, which is accompanied by the onset of superlattice reflections, corresponding to the tetragonal phase.

In the present description, two indexing schemes for the unit cell are used: one of them uses the cubic cell with dimensions $a_c = 4.191(1)$ Å and the other the tetragonal cell with $a = a_p\sqrt{2} = 5.903$ and $c = 2c_p = 8.384$ Å, where the subscript refers to the pseudocubic cell.

To obtain more information on the thermodynamic character of the transition, the integrated intensities of a set of eight of the strongest superstructure reflections of the type $(h + k) = 2n + 1$ and $l = 2n + 1$ were measured close to T_{c1} in the temperature range 150–210 K. Since the intensity of these reflections was much weaker than that of the normal ones, they were collected over a prolonged time (2 sec/step) in the ω scan mode.

The temperature variation of the unit cell parameters was measured using the X-ray powder technique on a Dron-type diffractometer (Cu$K\alpha$ radiation). The helium gas stream chamber maintained a temperature stabilization of 1 K. The evolution of the $(220)_c$ and $(400)_c$ profiles was modeled with Pearson VII functions to obtain their position and intensity. The other experimental details are given in Table 1.

TABLE 1
Details of Crystal Data, Data Collection, and Structure Refinement[a]

Crystal data			
Chemical formula	$K_{1-x}Li_xMnF_3$		
Temperature (K)	298		145
Formula weight	262.3		
Crystal system	cubic		tetragonal
Space group	*Pm3m*		*I4/mcm*
a (Å)	4.191(1)		5.903(1)
c (Å)			8.384(1)
V (Å)	73.61(2)		292.14(4)
Z	1		4
Sample dimens (mm)	$0.12 \times 0.13 \times 0.12$		
Density (calc) (Mg/m^3)	3.378		3.405
Absorption coeff μ (mm^{-1})	5.68		5.73
F(000)	70.4		281.4
Data Collection			
Radiation, wavelength (Å)	Mo$K\alpha$, 0.71073		
Monochromator	graphite		
No. of reflections for unit cell refinement	22		24
Scan type	ω–2θ		
2θ range (deg)	70		
Scan width (deg)	$1.0 + 0.3 \tan\theta$		
Index range	*h*: 0, 11		*h*: 0, 15
	k: 0, 11		*k*: 0, 15
	l: −11, 11		*l*: 0, 23
No. of reflections collected	1485		1238
No. independent reflections	184		571
F_o criterion	$\lvert F_o\rvert^2 \geq 2\sigma(F_o)^2$		
Corrections	Lorentz–polarization		
Standard reflections	2/50 measurements		
Decay of standards (%)	0.1		0.1
R_{int}	0.02		0.03
Refinement			
Refinement on	F^2		
No. of reflections used in ref	184		571
Number of varied parameters	6		11
Final R_1	0.021		0.045
Final *wR*	0.048		0.109
Godness of fit	1.353		1.037
Weight parameters c_1 and c_2	0.018, 0.01		0.0549, 1.74
Min, max residual (e $Å^{-3}$)	−0.78, 0.97,		−3.45, 2.07

[a] $R_{int} = \lvert F_o^2 - F_o^2(\text{mean})\rvert / \sum \lvert F_o^2\rvert$; $R_1 = \sum \lvert\lvert F_o\rvert - \lvert F_c\rvert\rvert / \sum \lvert F_o\rvert$; $wR = \{\sum\{w(F_o^2 - F_c^2)^2\} / \sum w(F_o^2)^2]\}^{1/2}$; $w = [\sigma^2(F_o^2) + (c_1P)^2 + c_2P]^{-1}$, where c_1 and c_2 are given in the table and $P = [(\max(F_o^2) + 2F_c^2)/3]$; Goodness-of-fit $S = [\sum w\lvert F_o - \lvert F_c\rvert / (n-m)]^{1/2}$, ($n$ = no of reflections, m = no. of parameters).

2. Structure Determination

2.1. Room temperature. At room temperature no distortion from the cubic system was observed. Thus the structure shown in Fig. 1 was refined in space group *Pm3m* with the site occupations given in Table 2. The distribution of K^+ and Li^+ over the shared site 1*a* was originally constrained to 0.96 and 0.04, respectively, according to the nominal value resulting from chemical analysis. The structural parameters were determined by full-matrix least-squares refinement on $|F^2|$. An empirical correction of $|F_c|$ for the isotropic extinction was calculated by refining the parameter x in the formula given in the program SHELXL93 (18): $k[1 + 0.001xF_c^2\lambda^3/\sin 2\theta]^{-1/4}$, where k is the overall scale factor. It appeared to be significant (Table 1) and reduces the conventional discrepancy factor R_1 from 0.068 to 0.046 due to the better fit of the low-angle

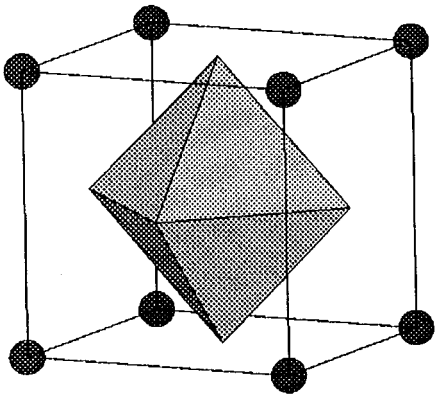

FIG. 1. Room temperature cubic structure of $K_{1-x}Li_xMnF_3$. The sites of the Mn ions are inside the octahedron formed by the F ions, with the K/Li ion at (0, 0, 0).

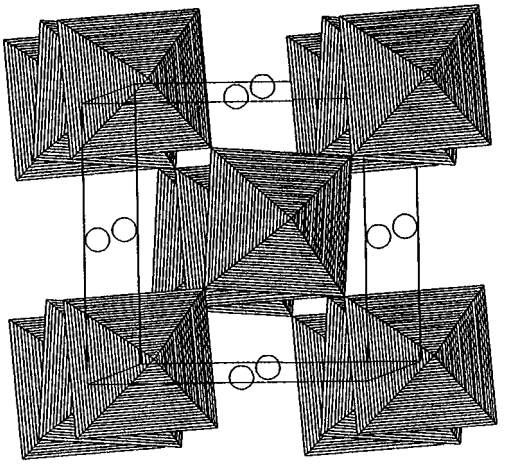

FIG. 2. Low-temperature tetragonal phase in the *I*4/*mcm* space group.

data. Such a severe extinction effect has also been observed in $KNiF_3$ (19) and $KCoF_3$ (20). Anisotropic refinement of the *F* atom further reduced the R_1 factor to 0.024. In the last stage of the structure calculations the site occupation factor for K^+/Li^+ was refined and converged to $x = 0.036(5)$. The final structural parameters are given in Table 2.

2.2. Low temperature (145 K). In the tetragonal phase below $T_{c1} = 191$ K, the structure is modified by octahedral tilting according to the classification $a^0a^0c^-$, following Glazer's notation (21, 22). The atomic displacements consist of correlated antiphase rotations of the octahedra about the [001] axis (Fig. 2). The structure at 145 K was refined in space group *I*4/*mcm* in analogy with the already known structure description for pure $KMnF_3$ (3). The final atomic coordinates and thermal vibration amplitudes are given in Table 3. Since the convergence of the anisotropic temperature factors for the K^+/Li^+ site was poor, in each refinement only the isotropic U_{eq} was considered physically significant for this site.

TABLE 2
Structural Parameters in the Cubic Phase (*Pm*3*m*)[a]

Atom	Site	U_{11}	U_{22}	U_{eq}	Site occupation factor
Mn	1*b* ($\frac{1}{2}, \frac{1}{2}, \frac{1}{2}$)	0.00797(6)		0.00797(6)	0.0208
K/Li	1*a* (0, 0, 0)	0.01976(11)			K: 0.0200
					Li: 0.0085
F	3*c* ($0, \frac{1}{2}, \frac{1}{2}$)	0.0080(3)	0.0369(5)	0.02725	0.0625

[a] The form of the anisotropic temperature factor is $T = \exp[-2\pi^2a^{*2}(h^2 + k^2 + l^2)U_{11}]$ for Mn and $\exp\{-2\pi^2a^{*2}[h^2U_{11} + (k^2 + l^2)U_{22}]\}$ for the F atom.

Atomic scattering factors for neutral atoms and corrections for anomalous dispersion were as in the SHELXL93 program (18), which was also used for all the structure calculations.

RESULTS AND DISCUSSION

At room temperature, the distribution of the isovalent K^+ and Li^+ ions at position 1*a* (0, 0, 0) was refined and found to be 0.964 and 0.036, respectively. The main feature of the structure is the high anisotropy of the amplitudes of the thermal vibrations of the F atom ($U_{33} = U_{22} > U_{11}$). A similar result has been obtained for pure $KMnF_3$ (23). Therefore, it cannot be associated with the presence of Li^+ substituents. It appeared also that static disorder resulting from nonuniform periodicity of the crystal lattice at the K/Li positions does not influence the K^+–F^- and

TABLE 3
Atomic Coordinates and Thermal Vibration Amplitudes U_{ii} in the Tetragonal Phase (145 K)

Atom	Site	U_{11}	U_{33}	U_{eq}	Site occupation factor
Mn	4*c* (0, 0, 0)	0.00544(8)	0.0057(10)	0.00554(7)	0.125
K/Li	4*b* ($\frac{1}{2}$, 0, $\frac{1}{4}$)			0.0115(1)	K: 0.120
					Li: 0.005
F(1)	4*a* (0, 0, $\frac{1}{4}$)	0.035(1)	0.0067(6)	0.0253(7)	0.125
F(2)	8*h* (x, $\frac{1}{2} + x$, 0)	0.0125(4)	0.0317(10)	0.0189(4)	0.250
	$x = 0.2675(3)$				

[a] The temperature factors are given by $T = \exp\{-2\pi^2a^{*2}[(h^2 + k^2)U_{11} + l^2c^{*2}U_{33}]\}$ and $U_{eq} = \frac{1}{3}(2U_{11} + U_{33})$.

TABLE 4
Selected Bond Distances (Å) at Room Temperature (RT) and at 145 K[a]

	RT	145 K	
Mn–F(1)	2.095 (1)	2.096(0)	2×
Mn–F(2)		2.0925(13)	4×
Mn–K	3.630(1)	3.620(1)	6×
F(1)–F(2)	2.963(1)	2.961(0)	4×
F(2)–F(2)$_i$		2.959(1)	4×
K–F(1)	2.963(1)	2.951(0)	4×
K–F(2)		2.856(2)	4×
K–F(2)$_i$		3.063(2	4×

[a]Symmetry code: (i) $y, -x, -z$.

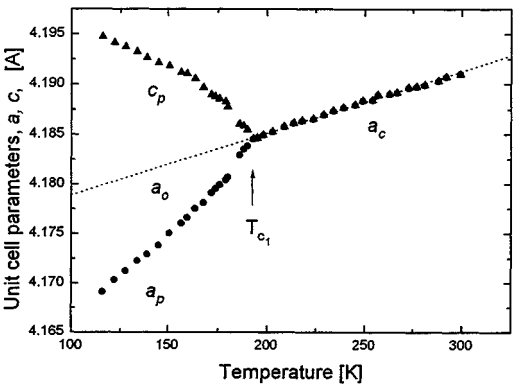

FIG. 3. Temperature variation of the unit cell parameters of a $K_{1-x}Li_xMnF_3$ single crystal.

Mn^{2+}–F^- distances (Table 4) when compared to the values for $KMnF_3$. Also, in the tetragonal phase at 145 K there is almost no difference between the Mn–F(1) and Mn–F(2) bond distances (Table 4). This means that the MnF_6 octahedra are essentially regular and rotate as rigid units. The K^+/Li^+ ions are not displaced from their position, although some difficulty in the refinement of their anisotropic thermal displacements may point to some site disorder. Unfortunately, the precision of the present experiment, limited by insufficient temperature stabilization, did not allow us to trace this effect in more detail.

To explain these observations one should refer to the cluster model used by Hutton *et al.* (24, 25) in describing the cubic–tetragonal transition in ABX_3 perovskites. The model is based on high-resolution studies of the elastic neutron diffraction for $SrTiO_3$, $KMnF_3$, $RbCaF_3$, and $CsPbCl_3$, which show strong anharmonic thermal vibrations of X^- ions already in the cubic phase. The cluster model assumes the crystal consisting of tetragonal microdomains with BX_6 octahedra distorted along each cubic axis, of which each one is equally probable. In a macroscopic sense, the crystal will have only statistically cubic symmetry. Regarding the X-ray diffraction, the ions in the crystal would appear to have large amplitudes of the thermal displacements. This is the case observed not only in $KMnF_3$ but also in $SrTiO_3$, $RbCaF_3$, and $CsPbCl_3$.

The Mn^{2+} cation with the d^5 electronic configuration is not Jahn–Teller active, no transition of that type can be expected. However, the observed F^- ion displacements at low temperature may cause a deformation of the Mn^{2+} high- symmetry electron distribution (half-filled d orbital) and there may also be some covalent contribution added to the predominantly ionic character of the Mn^{2+}–F^- bonds (26). The role of covalent bonding in anharmonicity close to the phase transition was pointed out by Megaw (27) and Weirich *et al.* (28). It is known that the principal cause of anharmonicity is any disorder of the structure arising from, for example, nonuniform periodicity of the crystal lattice. The size effect resulting from the difference in ionic radii of K^+ and Li^+ will enhance the local strain. Using the temperature dependence of the unit cell parameters close to T_{c1} (Fig. 3), we calculated the tetragonal deformation (Fig. 4) and the macroscopic strain. Above 191 K the cubic structure shows a linear thermal expansion behavior. The components $\{x_i\}$ of the macroscopic spontaneous strain in the tetragonal phase are $x_1 = x_2 = (a - a_0)/a_0$ and $x_3 = (c - a_0)/a_0$, where a_0 is the equivalent lattice constant of the cubic phase extrapolated to the same temperature conditions for which a and c are measured (29). It is clear from Fig. 5 that the macroscopic strain is anisotropic; the components x_1 and x_3 differ in magnitude and are of the opposite sign as the temperature is lowered.

The transition temperature was monitored by careful observation of temperature variation of the integrated intensities of the superstructure reflections. Results for the (123) and (231) reflections are shown in Fig. 6. This temperature dependence is regarded as the order parameter η (9, 12), which is expected to vary with temperature as $J \sim \eta \sim |T - T_{c1}|^{2\beta}$. It was not possible to observe the true

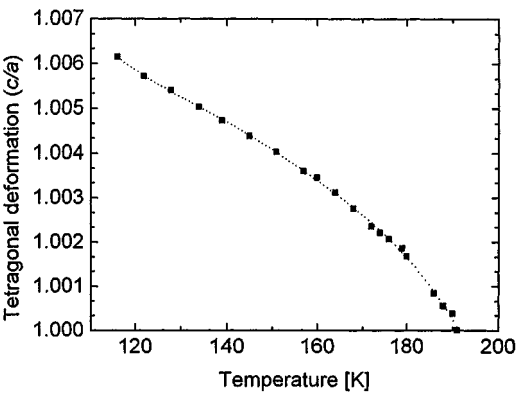

FIG. 4. Evolution of the tetragonal deformation (c/a) below T_{c1}.

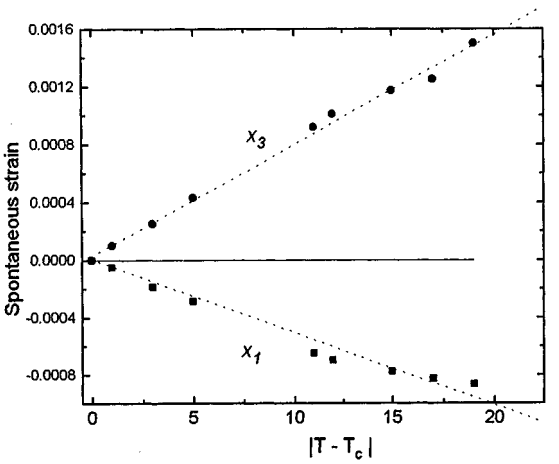

FIG. 5. Macroscopic spontaneous strain components $\{x_1$ and $x_3\}$ versus $|T - T_{c1}|$. The dashed line represents the best linear fit of the data for $T_{c1} = 191.2$ K.

character of the transition in the narrow critical region because of insufficient temperature stability; therefore we have not attempted to calculate the critical exponent. As the weak first-order nature of the transition resembles very much the observations by Shirane *et al.* in $KMnF_3$ (7), with the critical exponent $\beta \approx 0.24$, and because similar indication results from the spontaneous strain, then, assuming $\beta = 0.24$, we have obtained the transition temperature $T_{c1} = 191.2(4)$ K. This value matches the value resulting from the temperature variation of the unit cell and the corresponding relationships shown in Figs. 4 and 5. However, it was pointed out in ref 8 that experimentally determined β values are often much lower ($\beta \approx 0.25$ in refs 4, 10, and 11) than those expected from the $n = 3$ Heisenberg model with $\beta \approx 0.367$. The explanation for this discrepancy arises from the first-order character of the transition, which does not allow easy access to the critical region. On the other hand, the nature of the transition at T_{c1} is influenced by the domain structure, causing the critical region to be smeared out (12). In our experiment the domain structure is manifested as a residual intensity at the superlattice Bragg positions above T_{c1}. The resulting hysteresis is not higher than 2 K; i.e., it is slightly smaller than in $KMnF_3$ (3.6 ± 3 K). Since the domain structure is stabilized by the lattice defects, one can conclude that the Li^+ impurities weaken the first-order character of the transittion at T_{c1}.

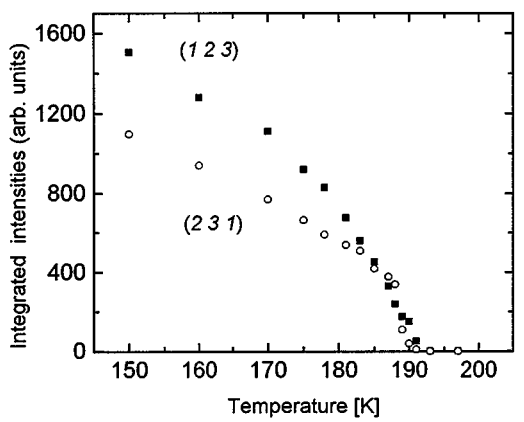

FIG. 6. Temperature dependence of the intensity of the superstructure reflections (123) and (231).

CONCLUSIONS

1. The cubic-to-tetragonal ($c/a > 1$) transition temperature is enhanced from $T_{c1} = 186$ K in the parent $KMnF_3$ to 191.2 K in $K_{1-x}Li_xMnF_3$ ($x = 0.036$).

2. At room temperature no "macroscopic" distortions from the cubic system were observed. The highly anisotropic thermal displacement amplitudes for the F^- ion are the main result of the structural refinement. This could not be attributed, however, to the Li^+ substituents because a similar effect has been observed in other perovskites of the $SrTiO_3$ type. Below T_{c1} the crystal lattice periodicity perturbation caused the local strains which force the F^- ions to move from their high- symmetry positions, and thus the low-symmetry phase is stabilized. The spontaneous macroscopic strain, enhancing the transition temperature, can be considered as an order parameter.

3. The thermodynamic nature of the transition does not change radically when compared to $KMnF_3$. For the fluctuation-driven, weakly first-order transition at T_{c1}, it was expected that the impurities introduced into the K^+ sites, would change the behavior to continuous. This was verified by measurements of the temperature dependence of the unit cell and the intensities of the superstructure reflections in the temperature range close to T_{c1}.

The effect of impurities on the structural distortion is much more pronounced if the substituents are introduced into the sites of the octahedra-centering Mn^{2+} ions. It was shown by Gibaud *et al.* (8) that the local strains induced by Ca^{2+} ions, with a larger ionic radius than that of Mn^{2+}, enhanced all three transition temperatures. The transitions at T_{c1} and T_{c2} were found to be especially sensitive to the Ca^{2+} concentration. The enhancement rates were 5.8, 18, and 14 K/at.% of Ca^{2+}, respectively. The interesting finding of these authors was that the temperature range of the orthorhombic phase III increased with the concentration of Ca^{2+} so that it would be possible to reach a crossover between the transitions at T_{c1} and T_{c2} at the extrapolated Ca^{2+} concentration, $x = 0.075$.

On the other hand, the introduction of Mg^{2+}, with a smaller ionic radius, in place of Mn^{2+} lowered T_{c1} and caused the transition to become continuous at the threshold concentration of Mg^{2+} ions (11). These results demonstrate that the crystal lattice imperfections at the octahedral sites,

leading to the perturbations in the B–F bond distances, influence the phase transitions in $KMnF_3$ in a more distinctive way than the impurities at the K^+ sites. However, in all cases the first-order character of the transition at T_{c1} becomes weakened.

REFERENCES

1. O. Beckman and K. Knox, *J. Phys.: Condens. Matter* **1,** 3565 (1989).
2. S. M. Shapiro, J. D. Axe, G. Shirane, and T. Riste, *Phys. Rev. B* **6,** 4332 (1972).
3. V. J. Minkiewicz and G. Shirane, *J. Phys. Soc. Jpn.* **26,** 674 (1969).
4. V. J. Minkiewicz, J. Fujii, and Y. Yamada, *J. Phys. Soc. Jpn.* **28,** 443 (1970).
5. M. Hidaka, N. Ohama, A. Okazaki, H. Sakashita, and S. Yamakawa, *Solid State Commun.* **16,** 1121 (1975).
6. H. Sakashita and N. Ohama, *Phase Transitions* **2,** 263 (1982).
7. G. Shirane, V. J. Minkiewicz, and A. Linz, *Solid State Commun.* **8,** 1941 (1970).
8. A. Gibaud, S. M. Shapiro, J. Nouet, and H. You, *Phys. Rev. B* **44,** 2437 (1991).
9. M. Hidaka, H. Fujii, and S. Maeda, *Phase Transitions* **6,** 101 (1986).
10. V. J. Nicholls and R. A. Cowley, *J. Phys. C*: *Solid State Phys.* **20,** 3417 (1987).
11. U. J. Cox, *J. Phys.: Condens. Matter* **1,** 3565 (1989).
12. U. J. Cox, A. Gibaud, and R. A. Cowley, *Phys. Rev. Lett.* **61,** 9 (1988)
13. A. Ratuszna, *J. Phys.: Condens. Matter* **5,** 841 (1983).
14. R. D. Shanon, *Acta Crystallogr., Sect. A* **32,** 751 (1976).
15. D. Skrzypek, P. Jakubowski, A. Ratuszna, and A. Chekowski, *J. Crystal Growth* **48,** 475 (1980).
16. Kuma Diffractiom Software, Version 8.1, Wrocław, Poland, 1995.
17. J. Cosier and A. M. Glazer, *J. Appl. Crystallogr.* **19,** 105 (1986).
18. G. M. Sheldrick, SHELXL 93: Program for the Refinement of Crystal Structures. University of Göttingen, Germany, 1993.
19. N. Kijima, K. Tanaka, and T. Marumo, *Acta Crystallogr., Sect. B* **37,** 545 (1981).
20. N. Kijima, K. Tanaka, and T. Marumo, *Acta Crystallogr., Sect. B* **39,** 557 (1983).
21. A. M. Glazer, *Acta Crystallogr., Sect. B* **28,** 3384 (1972).
22. A. M. Glazer, *Acta Crystallogr., Sect. B* **31,** 756 (1975).
23. S. Åsbrink and A. Waśkowska, *Eur. J. Solid State Inorg. Chem.* **31,** 747 (1994).
24. J. Hutton, R. J. Nelmes, G. M. Meyer, and V. R. Eiriksson, *J. Phys. C*: *Solid State Phys.* **12,** 5393 (1979).
25. J. Hutton and R. J. Nelmes, *J. Phys C*: *Solid State Phys.* **14,** 1713 (1981).
26. R. H. Buttner, E. N. Maslen, and N. Spadacini, *Acta Crystallogr., Sect. B* **48,** 639 (1992).
27. H. Megaw, *Acta Crystallogr.* **5,** 739 (1952).
28. K.-H. Weirich and R. Siems, *Z. Phys. B* **61,** 63 (1985).
29. E. K. H. Salje, *Acta Crystallogr., Sect. A* **47,** 453 (1991).